



OPEN

## A novel development of wide voltage supply DC–DC converter for fuel stack application with PSO-ANFIS MPPT controller

C. H. Hussaian Basha<sup>1✉</sup> & Faisal Alsaif<sup>2</sup>

The present power production companies are working on renewable energy systems because their features are more reliable for the local energy consumers, high continuity in the energy production, and less cost is required for maintenance. In this article, the proton exchange membrane fuel stack (PEMFS) renewable energy is utilized to supply energy to the automotive systems. Here, the PEMFS is selected because of its merits are high energy density, quick system response concerning the source operational temperature, and more suitable for electric vehicle application. However, the PEMFS supplied voltage is completely nonlinear which is solved by utilizing the modified particle swarm optimization with adaptive neuro-fuzzy inference system (MPSO with ANFIS) controller. This hybridization-based maximum power point tracking controller provides more accuracy, high power point identifying speed, best dynamic response at different fuel stack functioning temperature conditions, and easy maintenance. Here, the fuel stack generated current is very high which is optimized by introducing the new DC–DC converter. The advantages of this DC–DC converter are more voltage transformation ratio, low-level voltage stress appearing across the switches, and wide voltage gain. The overall system is investigated by utilizing the MATLAB/Simulink tool.

**Keywords** Boost DC–DC circuit, Duty value, Efficiency of MPPT, Fast tracking speed of MPP, Good reliability of the system, Quick system response

### Abbreviations

MPSO	Modified particle swarm optimization
ANFIS	Adaptive neuro-fuzzy inference system
CSO	Cuckoo search optimization
MPPT	Maximum power point tracking controller
MPP	Maximum power point
PEMFS	Proton exchange membrane fuel stack
SOFS	Solide oxide fuel stack
MCFS	Molten carbonate fuel stack
AVSV-P&O	Advanced variable step value based perturb & observe
ASB-FLC	Adaptive step based fuzzy logic controller
MSL-PSO	Modified step length based PSO
ALV-CSO	Adjustable levy value of cuckoo search optimization
AFS	Alkaline fuel stack
PAFS	Phosphoric acid fuel stack

The usage of conventional energy supply networks is reduced because of its disadvantages are high implementation cost, more cost needed for running the power supply network, high human source necessity, excessive atmospheric effects, high amount of nitrous oxide release in the environment, and low level of reliability for the urban power consumers<sup>1</sup>. In the article<sup>2</sup>, the authors discussed the thermal energy supply which is utilized for the battery storage application. The features of this thermal system are a backup power supply, cooling alternatives,

<sup>1</sup>Department of Electrical and Electronics Engineering, SR University, Hanumakonda, Telangana 506371, India. <sup>2</sup>Department of Electrical Engineering, College of Engineering, King Saud University, 11421 Riyadh, Saudi Arabia. ✉email: sbasha238@gmail.com

and efficient heating. However, the disadvantages of these thermal networks are enormous volumes of pollutants affect the atmospheric conditions. So, the scholars developing advanced renewable systems for optimizing the environmental pollutants and providing the backup power for the emergency hospitalized applications<sup>3</sup>. The renewable energy supply networks are classified as biomass, hydrogen, wind energy, tidal power, sunlight energy, and hydroelectricity. Biomass energy production systems utilize biological waste materials for producing useful electricity. Here, agriculture wastage, and residue are also considered in the biomass systems<sup>4</sup>. The features of biomass networks are high abundance, zero level carbon footprint, minimized usage of fossil fuel quantity, more affordable than fossil fuels, and less landfill wastage. However, the disadvantages of biomass networks are highly expensive when associated with solar, high space, moderate greenhouse gas emissions when compared to the thermal energy sources, and more environmental impact<sup>5–7</sup>.

The hydroelectricity network is implemented in the hilly areas because this system requires a high amount of water head for running the turbine. At medium and low water head levels, the hydraulic energy networks give very less efficient energy to the consumers<sup>8</sup>. So, the hydro networks are installed at the water availability space. The features of these hydroelectric systems are clean energy, relatively more efficient, and highly useful for different automotive applications. Also, this system is used in many applications which are flood control, drinking water purposes, milling, grinding, and irrigation applications. The drawbacks of this system are unmanaged dams, more environmental impacts, destruction of natural resources, droughts, and impact on fish life<sup>9</sup>. So, the tidal energy sources are used for the crushing of grains. Also, it helps to store the energy in the form of hydroelectric dams. Here, the tidal wave energy is transferred to electrical power for household systems. The natural tidal waves rise and fall completely based on the gravitational interaction between the moon, sun, and earth<sup>10</sup>. The features of tidal networks are less carbon emissions, more predictable, and good energy output. However, the tidal network construction takes more development costs, more negative impacts on marine life, limited locations, and variable intensity of waves<sup>11</sup>.

The drawbacks of tidal systems are limited by utilizing windmills. In the article<sup>12</sup>, the scholars expressed the wind energy systems for drinking water pumping applications. Also, it is applied for irrigation forms to reduce electricity bills. In this, the wind blades collect the kinetic energy of the atmospheric air and it is transferred to the generator shaft for achieving the electrical energy. The features of wind networks are more reliability, less CO<sub>2</sub> emissions in nature, more safer energy source, no need to worry about fossil fuels consumption, and good efficiency<sup>13</sup>. The major demerits of wind networks are less suitable for all locations to install, more noise creation, and high visual effects. The disadvantages of windmills are compensated by utilizing the sunlight networks. The sunlight networks are installed in many places without any limitations. Also, it may not give any noise pollution or visual effects. The sunlight cells are implemented by utilizing the P and N category silicon semiconductor materials<sup>14</sup>. Here, the sunlight cells capture the solar insolation thereby the free electrons in the P-N material start energizing to move to the external load circuit. However, the solar system works effectively in the daytime only. So, the present electric vehicle industry utilizes the fuel stack technology for supplying electricity to the electric vehicle motor<sup>15</sup>.

From the literature study, the fuel stack technologies are differentiated based on the electrolyte availability in the network. In the article<sup>16</sup>, the scholars referred to the Alkaline Model Fuel Stack Technology for the military and satellite energy supply. Here, the H<sub>2</sub> fuel source is utilized at the anode, and the air oxidizer is used at the cathode to provide the energy to the external local consumers. The selected electrolyzed material in this stack is immobilized potassium hydroxide. The operational temperature of this fuel stack is 220 °C and its electrolyze gives 60% maximum efficiency. The advantages of this stack are low-cost electrolyte utilization, and fast system response because of the quick response of the cathode reaction. The major issue of the alkaline stack is electrolyte management difficulty<sup>17</sup>. So, the molten carbonate electrolyte-based fuel stack technology is considered in the article<sup>18</sup> for distributed power generation systems. In this stack, carbon monoxide, carbon dioxide, and hydrogen chemicals are utilized as the input fuels to this system for obtaining highly efficient electrical energy. The category of electrolyte used in this stack is immobilized molten carbonate liquid electrolyte. This stack works at the highest operational temperature which is equal to 650 °C. The features of this stack are more operational efficiency, high output electric utility, the ability to work with many catalyst materials, and high-level fuel flexibility<sup>19–22</sup>. However, the disadvantages of this fuel stack are high corrosion on electrodes and breakage of components. Also, this system gives less power density and utilizes more time for functioning.

To overcome the corrosion issues of molten carbonate material, a phosphoric acid-dependent fuel stack technology is developed in the article<sup>23</sup> for smart grid-based distribution power supply network applications. Here, the natural air and hydrogen components are working as an input fuel to this fuel module. The liquid phosphoric acid and silicon carbides are selected as electrolyte materials for enhancing the chemical reaction rate. The features of this fuel stack are capable of operating at high working temperature conditions and are highly tolerable for impure supply source fuels<sup>24</sup>. However, this fuel stack faces the challenges of long starting time, and more cost of platinum material is required for developing this fuel module. To overcome the disadvantages of the above fuel systems, a PEMFS is proposed in this work to provide highly efficient electricity to the electric vehicle systems. The features of this polymer membrane fuel stack are solid electrode usage for eliminating corrosion-related issues, fewer electrolyte-related issues, and fewer maintenance problems. Also, this fuel stack needs very low-level functioning time and is capable of working at any low-temperature conditions. The utilization of fuel module technology is defined in the Fig. 1.

The generated fuel module voltage is nonlinear fashion which makes the system provide low-level output power. So, to maximize the power supply of the fuel module, an MPPT controller is selected in the article<sup>26</sup> for enhancing the power supply rating of the proposed system thereby tracking the operational point of the source network. From the literature study, the MPPT technologies are differentiated as artificial intelligence, nature swarm intelligence, and conventional and machine learning controllers. The most frequent P&O methodology is considered in the article<sup>27</sup> for traffic signal monitoring applications. The features of this algorithm are very

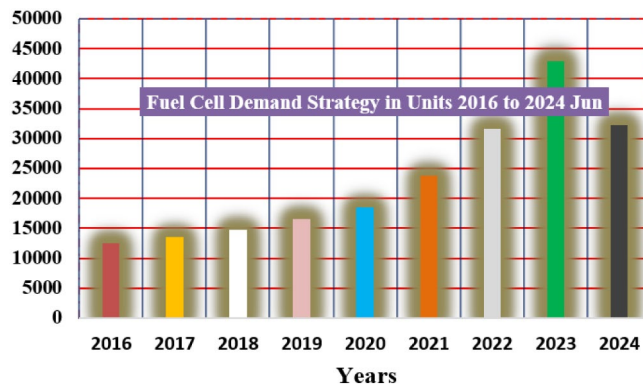


**Figure 1.** Overall fuel network utilization for electric vehicle systems<sup>25</sup>.

simple in design, good reliability of the technique, better understanding, and easy to handle. However, the disadvantages of this controller are more distortions of fuel stack supply voltage and a low level of MPP accuracy. The simplified IC technology is selected in the article<sup>28</sup> for solar, and fuel stack hybrid network-based water pumping systems. This controller collects the sunlight intensity, sun temperature, fuel stack hydrogen supply, and oxygen decomposition for evaluating the required duty of the quadratic interleaved converter. The cost of this network is more when associated with the P&O conventional controller. Also, this adaptive incremental conductance needs a high amount of time to find out the overall system's global operational point. So, the authors combined the IC with the Kalman filter technology for collecting the all-distorted sunlight and fuel stack source currents thereby obtaining the uniform load voltage for the consumer application<sup>29</sup>. Also, the IC-Kalman filter methodology helps for central grid to give energy to the automotive systems with a unity power factor. However, this type of conventional network struggles with the fuel system oscillations across MPP. In the article<sup>30</sup>, the scholars developed the sliding technology to identify the continuous disturbance of the hydrogen decomposition in the fuel module, and sunlight intensity variation in the hybrid fuel module and solar system. Here, there are two interleaved converter circuit technologies are applied to the two renewable energy systems to improve their output power extraction capability.

The features of slider axial tracking technology are more accuracy in MPP finding, more suitable duty cycle selection for the power transformation circuit, more suitable for any sunlight operational temperature conditions, easy to handle source fuel controlling of the fuel module, and better robustness. However, the sliders do not provide the exact MPP location of the fuel module-based smart grid power production network. So, the Incremental Resistive power point identifier is selected in the article<sup>31</sup> for enhancing the fuel stack source power density thereby giving the uniform source voltage to the hydrogen-dependent electric vehicles. The features of this incremental resistive controller are easy to understand, and more useful for static fuel stack working temperature conditions. However, the disadvantages of the above methods are less applicable for the quick variation of the fuel stack network. So, in this work, an MPSPSO with ANFIS controller is developed for the polymer membrane fuel stack network for identifying the exact MPP location. Here, the hybridization concept is introduced in the proposed system to improve the fuel stack efficiency, quick system dynamic response, and robustness. The introduced modified hybrid MPPT block is given in Fig. 2.

From Fig. 2, the fuel stack supplied voltage level is very low which can be improved by applying the power electronics DC-DC circuit. From the literature review, the DC-DC circuits are differentiated based on the interfacing of rectifier circuits which are transformer-dependent DC-DC networks, and non-isolation-based boost DC-DC circuits. The transformer includes power transformation circuits flyback circuits, full bridge circuits, half-bridge circuits, and feedforward power converter<sup>32</sup>. These isolated circuits utilize the transformers to create the separation between the source circuit and the load circuit. Also, it requires the rectifier power electronic device for transferring the continuous AC source to the DC source. In the article<sup>33</sup>, the scholars referred to the flyback technology in the DC-DC circuit for telecommunication applications. The features of this technology are the high ability to give galvanic isolation and automatic handling of reactive and real powers. However, the drawbacks of this flyback technology are high current ripples, excessive noise generation, lower power transformation efficiency, more complexity in circuit design, and higher peak voltages on the switches. Also, it can not provide higher power density to the system<sup>34</sup>. So, the full bridge technology-dependent power circuit is selected for running the induction motor drives. The merits of this converter are the ability to supply more output voltage and gives maximum possible efficiency. But it takes more development cost and requires more power switches<sup>35</sup>. In this article, a wide power supply-based single switch power transformation circuit is developed to improve the voltage supply capability of the fuel module network. The features of this introduced converter are a low level of voltage stress across the switches, a better voltage transformation ratio, and low implementation cost.

### Mathematical development of PEM fuel stack

Fuel stack technology is a very fast-growing application for hydrogen-dependent automotive systems. In the article<sup>36</sup>, the authors developed the solid oxide electrolyte-based fuel stack for auxiliary power supply applications. Also, it is used for electric utility and distributed power supply applications. However, this solid oxide creates corrosion-related issues. As a result, the entire developed system's operational efficiency is reduced<sup>37</sup>. In

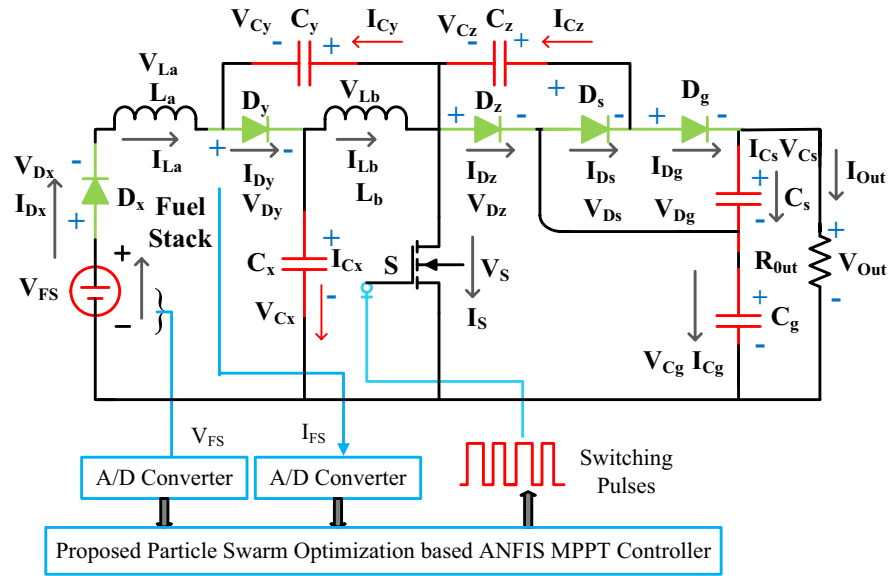


**Figure 2.** MPSTO with ANFIS fed Single Switch DC–DC circuit for PEMFS.

this article, the polymer membrane electrolyte-dependent fuel stack is proposed for hydrogen-powered electric vehicle systems. The operational structure and the electrical current flow of the PEM fuel module are represented in Fig. 3a, and b. The features of this selected fuel stack are more efficiency, less corrosion-related issues, less electrolyte handling problems, and the ability to function at low- and high-level operational temperature conditions. Also, it starts working with very little time. Due to this condition, the polymer membrane fuel stack is used for automotive large vehicle applications. Also, the polymer membrane-dependent fuel stack is interfaced with the smart grid-based standalone system for energy supply to the large vehicle networks for transportation applications.

From Fig. 3a, the fuel stack consumed source fuels are natural air,  $O_2$ , and  $H_2$ . At the anode, the hydrogen element is transferred to a small number of ions thereby the electrons follow the external utilized load circuit for giving the electrical source to the power transformation circuits. Similarly, the oxygen atoms release the positive charge ions which are added with the hydrogen atoms for releasing the output water content. Here, the hydrated polymer material electrolyte helps to improve the electron flow in the fuel stack and it has the property of zero corrosion-related issues, and the ability to withstand high operational fuel stack temperature conditions. However, the major challenge of this fuel stack is a more expensive catalyst and very low sensitivity with the impure supply fuels. The chemical reaction formation of the utilized fuel network is mentioned in Eqs. (1), and (3). From Eq. (1), the single polymer fuel cell provides only 1.2 V which is quite low-level voltage and it is not helpful for heavy-duty electric vehicle application. So, there are “n” cells selected for reaching the peak electricity demand.

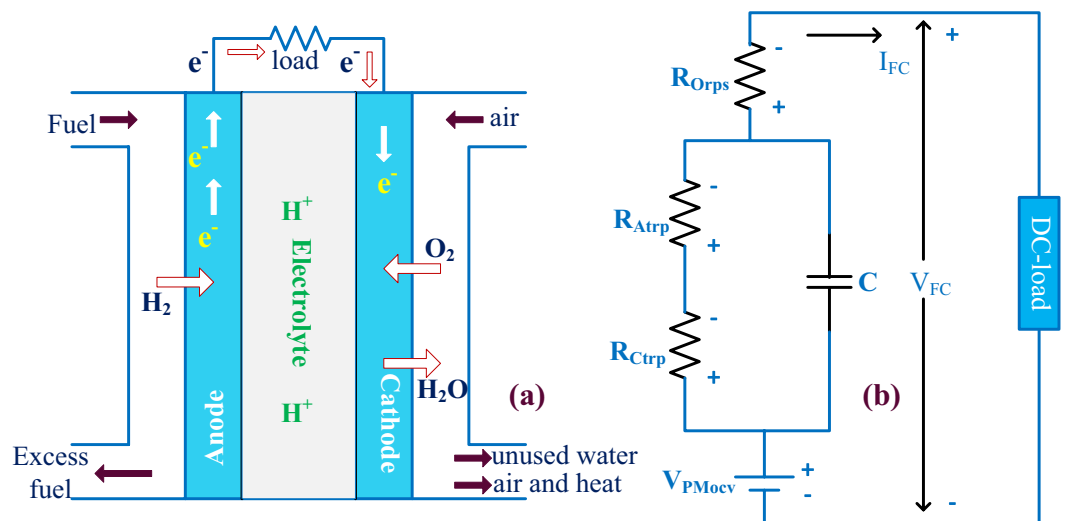
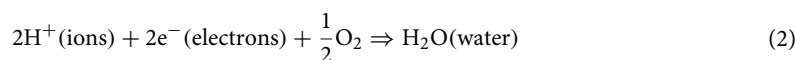
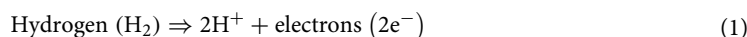


**Figure 3.** (a) Structure of polymer membrane-based fuel system, and (b) its electrical voltage flow.



$$\text{Energy}_{\text{Total}} = n (\text{total cells}) * V_{\text{FC}} \quad (4)$$

$$V_{\text{FC}} = V_{\text{PMocv}} - V_{\text{Orps}} - V_{\text{Atrp}} - V_{\text{Ctrp}} \quad (5)$$

$$E_{\text{PMocv}} = 1.29 - 0.786e^{-3} * (T_{\text{PFs}} - 299.781) + 3.989e^{-5} \log(P_{\text{H}_2} \sqrt{P_{\text{O}_2}}) T_{\text{PFs}} \quad (6)$$

$$P_{\text{H}_2} = \frac{1}{2} \text{RH}_{\text{Fsa}} * P_{\text{H}_2\text{O}}^s \left( \frac{1}{\frac{\text{RH}_{\text{Fsa}} P_{\text{H}_2\text{O}}^s}{P_{\text{Fsa}}} \exp\left(\frac{1.6 \left(\frac{I_{\text{cell}}}{\text{Area}}\right)}{T_{\text{PFs}}}\right)} \right) \quad (7)$$

$$P_{\text{O}_2} = \frac{1}{2} \text{RH}_{\text{Fsc}} * P_{\text{H}_2\text{O}}^s \left( \frac{1}{\frac{\text{RH}_{\text{Fsc}} P_{\text{H}_2\text{O}}^s}{P_{\text{Fsc}}} \exp\left(\frac{4.214 \left(\frac{I_{\text{cell}}}{\text{Area}}\right)}{1.564 * T_{\text{PFs}}}\right)} \right) \quad (8)$$

where the constraints  $V_{\text{PMocv}}$ ,  $V_{\text{Orps}}$ ,  $V_{\text{Atrp}}$ , and  $V_{\text{Ctrp}}$  are fuel network open-circuited potential, ohmic region-related voltage loss, active polarization-based voltage loss, and electron concentrative voltage loss. Here, the fuel stack voltage is determined by applying the Nernst concept which is mentioned in Eq. (6). The parameters  $P_{\text{H}_2}$ , and  $P_{\text{O}_2}$  are determined as partially generated  $\text{H}_2$ , and  $\text{O}_2$  pressures. The relative humidity values of the fuel system anode side and cathode chamber are  $\text{RH}_{\text{Fsa}}$ , and  $\text{RH}_{\text{Fsc}}$ . Here, the electrode's produced pressures are  $P_{\text{Fsa}}$ , and  $P_{\text{Fsc}}$ . The fuel system development has been made by considering the Table 1 parameter. The fuel system produced current and power curves are mentioned in Fig. 4a, and b.

## Development and analysis of power point tracking controllers

From the literature study, all of the fuel stack and renewable technologies provide nonlinear currents. Due to this issue, most of the solid oxide and polymer membrane materials-based fuel systems generate very little energy<sup>38</sup>. Also, the hydrogen power transformation efficiency of the fuel systems is less than 60%. So, the maximum power point identifiers are utilized for capturing the high amount of hydrogen energy thereby reducing the source oxygen and hydrogen utilization. Here, the Modified Particle Swarm Optimization with adaptive neuro-fuzzy inference system (MPSO with ANFIS) controller is developed to extract the maximum possible peak power of the fuel network. The proposed MPSO with ANFIS hybrid controller is analyzed along with the advanced variable step value based perturb & observe (AVSV-P&O), adaptive step based fuzzy logic controller (ASBFLC), modified step length based PSO (MSL-PSO), and adjustable levy value of cuckoo search optimization (ALV-CSO). Also, the developed and proposed MPPT controller comprehensive analysis has been done in terms of MPPT

Variable name	Values
Selected base generated power value of the fuel system ( $P_{\text{peak}}$ )	1.260 k Watts
Overall network production voltage in the fuel system ( $V_{\text{Peak}}$ )	24.23Volts
Peak current produced from the polymer membrane fuel stack ( $I_{\text{Peak}}$ )	52A
Overall air passing rate in the polymer membrane stack ( $I_{\text{pm}}$ )	419.897
Polymer membrane electrolyte generated gas constant value (R)	83.28956 [J mol <sup>-1</sup> K <sup>-1</sup> ]
Determined polymer membrane material Faraday constant (F)	91,624.5675 [C mol <sup>-1</sup> ]
Oxygen reaction-based composition value for the polymer membrane	22.256%
The entire fuel utilization of the proposed polymer membrane stack	98.672%
$\text{H}_2$ reaction decomposition rate for polymer membrane stack	98.891%
$\text{O}_2$ reaction decomposition rate for polymer membrane stack	66.785%

**Table 1.** Utilized polymer membrane development values for automotive networks.

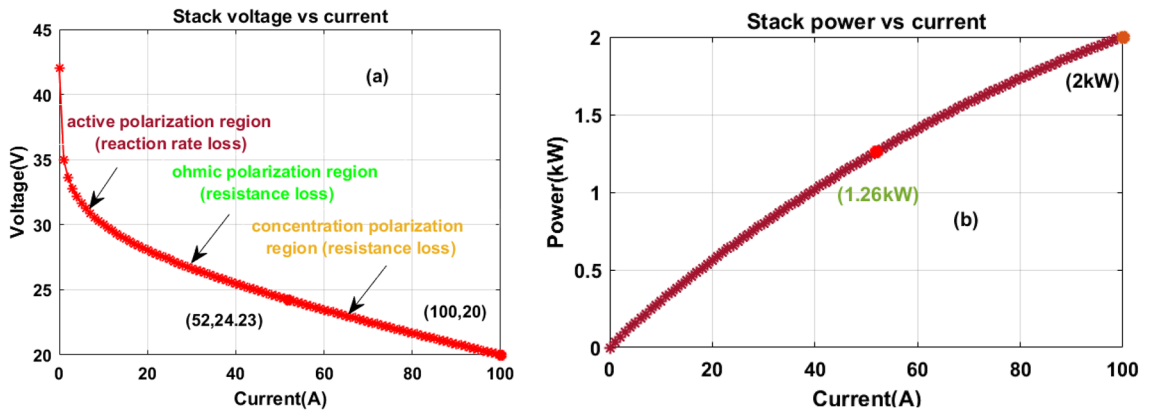


**Figure 4.** (a) The current curve of the polymer electrolyte fuel system. (b) The power curve of the polymer electrolyte fuel system.

finding accuracy, settled time of the operational point of selected fuel stack, convergence rate of the controller, and distortions of the converter power.

**Advanced variable step value-based perturb and observe**

The P&O technology is a very general and commonly applied power point identifier for most of the non-conventional power production networks because of its unique features are less implementation cost, very easy to understand, better static power response, and more suitable for traffic control networks<sup>39</sup>. However, this methodology takes more convergence rate for continuous change of the fuel system hydrogen pressure. So, the variable value step-based perturb and observe concept is utilized in the article<sup>40</sup> for improving the power production capability of the sunlight, and battery-fed solid oxide fuel system. In this hybridization solar and battery system, the battery charging life, and its depth of discharge are selected for supplying the duty waveforms for the quadratic Z-source dual switches DC-DC circuit. From Fig. 5, the duty of the quadratic circuit is adjusted positively when the functioning point of the fuel system is at its origin place. Later, the duty signals strength is optimized for identifying the natural MPP place as given in Eqs. (9), and (10).

$$\Psi(U) = \Psi(U - 1) + \psi * \left( \frac{P(U) - P(U - 1)}{V(U) - V(U - 1)} \right) \tag{9}$$

$$\Psi(U) = \Psi(U - 1) - \psi * \left( \frac{P(U) - P(U - 1)}{V(U) - V(U - 1)} \right) \tag{10}$$

From Fig. 5, the variables  $\Psi$ , P, and V are the utilized converter duty signal, power, and current of the fuel stack. Here, the variable  $\psi$  is the step value of the applied power point tracking controller.

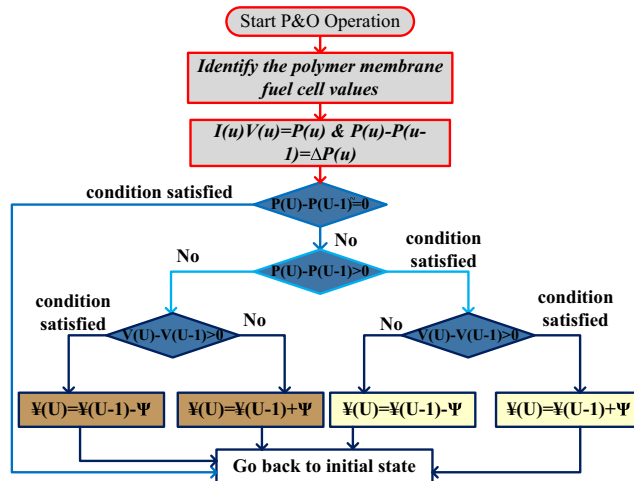


**Figure 5.** Advanced variable step value-based perturb and observe controller.



### Adaptive-step-based fuzzy logic controller for PEM fuel stack

The updated conventional methodologies are facing the troubles of distortions in the system power. Also, it cannot find out the exact operational position of the polymer fuel power production network<sup>41</sup>. So, the artificial intelligence technologies are showing better results when associated with the P&O and incremental resistance power point identifiers. In the article<sup>42</sup>, the researchers referred to the neural technology for collecting the wind and fuel stack integrated battery signals for running the whole microgrid network with uniform supply voltage. Here, the neural structure is big because of the greater number of source signals. As a result, the convergence rate of the whole system is reduced and its associated training time is more. Also, the neural controller topology provides a very low level of efficiency. So, the fuzzy technology is selected in the article<sup>43</sup> for the identification of the operational point of the hybrid renewable energy system. The most popular applications of fuzzy systems are easy target identification, pattern recognition, and decision-making in heavy-duty hydrogen vehicles. The implemented structure of the fuzzy technology is mentioned in Fig. 6. From Fig. 6, the fuel network supplied peak power error and its adjustment of error is sent to the fuzzification block for obtaining the required duty value of the DC–DC converter. The peak voltage error ( $e(q)$ ), and variable in its error value ( $\Delta e(q-1)$ ) are mentioned in Eq. (11).

$$e(q) = \frac{P(q) - P(q-1)}{V(q) - V(q-1)}; \Delta e(q) = e(q) - e(q-1) \tag{11}$$

### Modified step length-based PSO MPPT controller

The most utilized optimization controller is the particle swarm controller because its merits are very simple, with no need for mathematical derivations, and its functioning efficiency is more based on population utilization<sup>44</sup>. However, the PSO faces issues are moderate convergence speed, less accuracy for multidimensional problems, and takes high level of iteration value. So, the authors utilized a modified swarm controller for the heavy-duty electric vehicle-fed polymer membrane-based fuel stack network. Here, most of the particle agents are initiated by utilizing the different random weights. At the starting stage of the swarm intelligence, the agents go in various directions with various velocity values for catching the fuel stack operational point<sup>45</sup>. After that, the agents complete a certain number of iterations to move towards the actual target value. The selection of agents depends on the type of nonlinear issue of the proposed polymer fuel stack network. The agent’s velocities and their moving positions are upgraded by utilizing Eqs. (12), and (13). From Eq. (12), the PSO tries to capture the maximum possible peak power by selecting the differential slope step of the PEMFS P–I curve<sup>46</sup>.

$$V^{d+1} = V_c^d * W + g_1 q_1 (P_{best\_c} - x_c^d) + g_2 q_2 (G_{best\_c} - U_c^d) \tag{12}$$

$$U^{d+1} = U_c^d + V_c^{d+1} \tag{13}$$

where the generally available peak power position is  $P_{best}$ , and the required fuel stack peak power position is identified as  $G_{best}$ . The particles’ running velocity and their associated places are represented as  $V$ , and  $U$ . From Eq. (13), and Fig. 7, the starting particles position is too long when equated with the other agents. Later, the agents go in uniform directions with high accuracy.

### Adjustable levy value of cuckoo search dependent MPPT controller

The cuckoo search methodology is completely dependent on the metaheuristic network and it is developed from the natural behavior of the cuckoo movements. The features of the cuckoo algorithm are more superiority for

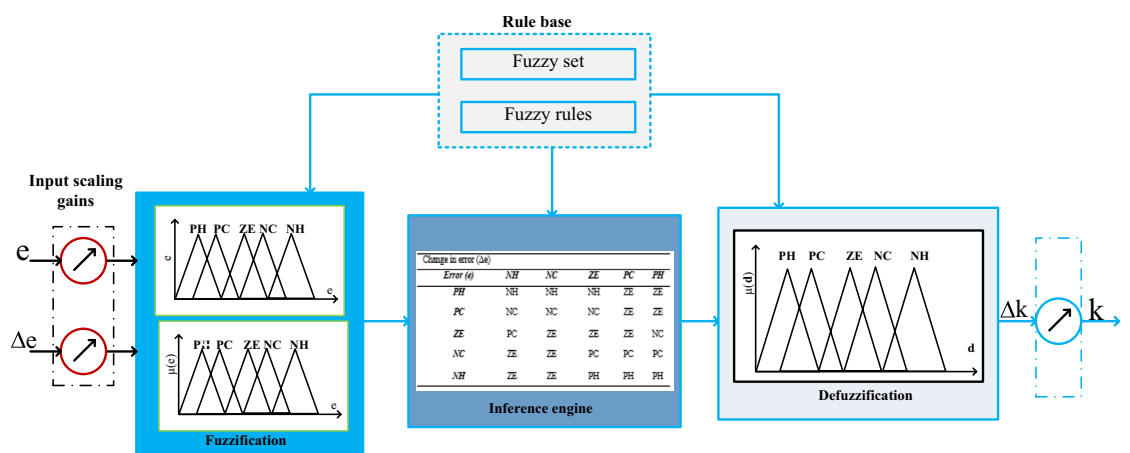
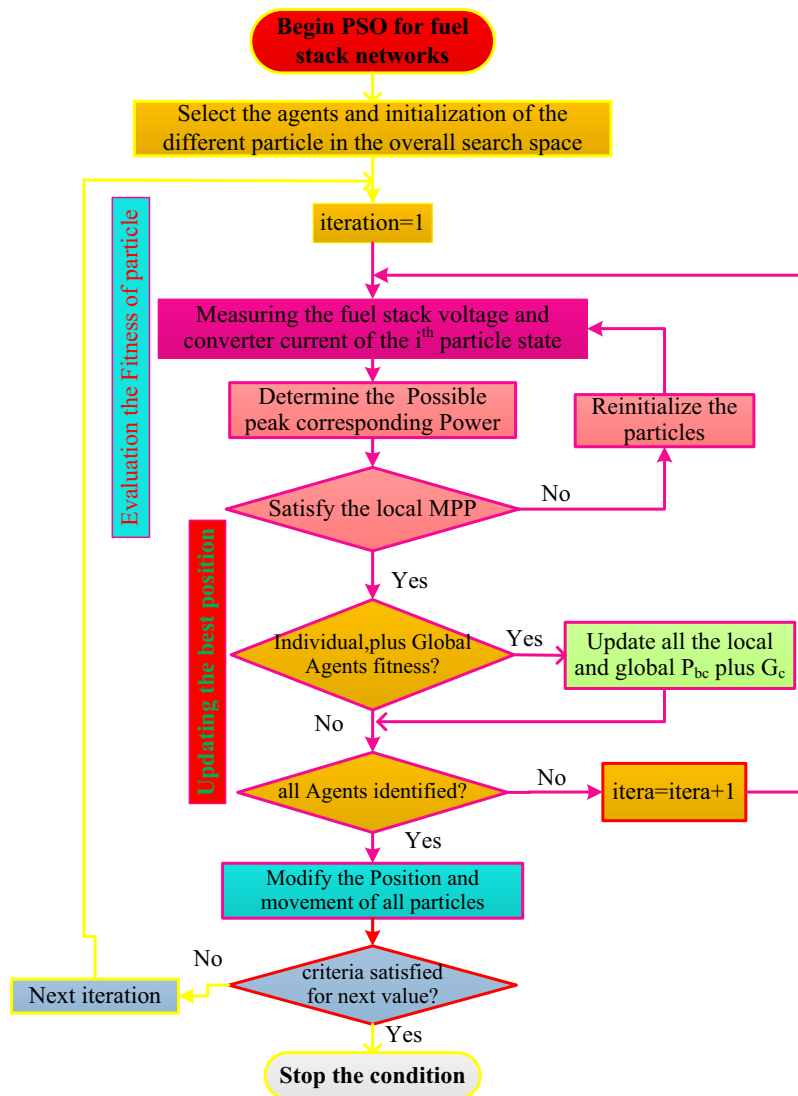


Figure 6. Applied fuzzy block to the polymer membrane-based fuel power system.



**Figure 7.** Modified step length PSO-dependent MPPT controller.

handling high complexity nonlinear issues, more simplicity when associated with the state algorithms, the ability to work with very small length levy value, better implementation, and more accuracy. However, this algorithm faces the issues of being unable to handle more complex search space, less utility for multidimensional issues, and less potential premature convergence. So, the scholars refer to the adjustable levy-dependent cuckoo network for achieving the maximum possible output power from the solar, and fuel stack-fed automotive system. In this methodology, the algorithm captures the sunlight intensity, cell temperature, and fuel network hydrogen decomposition to find the exact position of the fuel stack functioning point. The developed structure of this cuckoo system is illustrated in Fig. 8. From Fig. 8, the cuckoo works depending on the three logical rules which are every cuckoo provides only a single egg. In the second logical function, the available objectives in the initial iteration should have very good-quality cuckoo eggs. Finally, the host cuckoo's nest objectives are constant.

$$\text{Levy}(\Omega) = L^{-\Omega} 0.978 < \Omega < 3.556 \tag{14}$$

$$y_q^{u+1} = y_q^u + \psi \oplus \text{levy}(\Omega) \tag{15}$$

where the  $\Omega$  and  $y$  are the cuckoo's operational constants and its associated position. Here  $\psi$  is the utilized step constant for identifying the exact place of the Cuckoo network.

**Modified particle swarm optimization with adaptive neuro-fuzzy inference system**

The unique cuckoos and swarm intelligence methodologies face the problems of more number iterations count and excessive convergence speed fall, low-level accuracy, and not being useful for multidimensional complex issues. Also, the neuro methodologies take a high amount of convergence time for training the complex data of



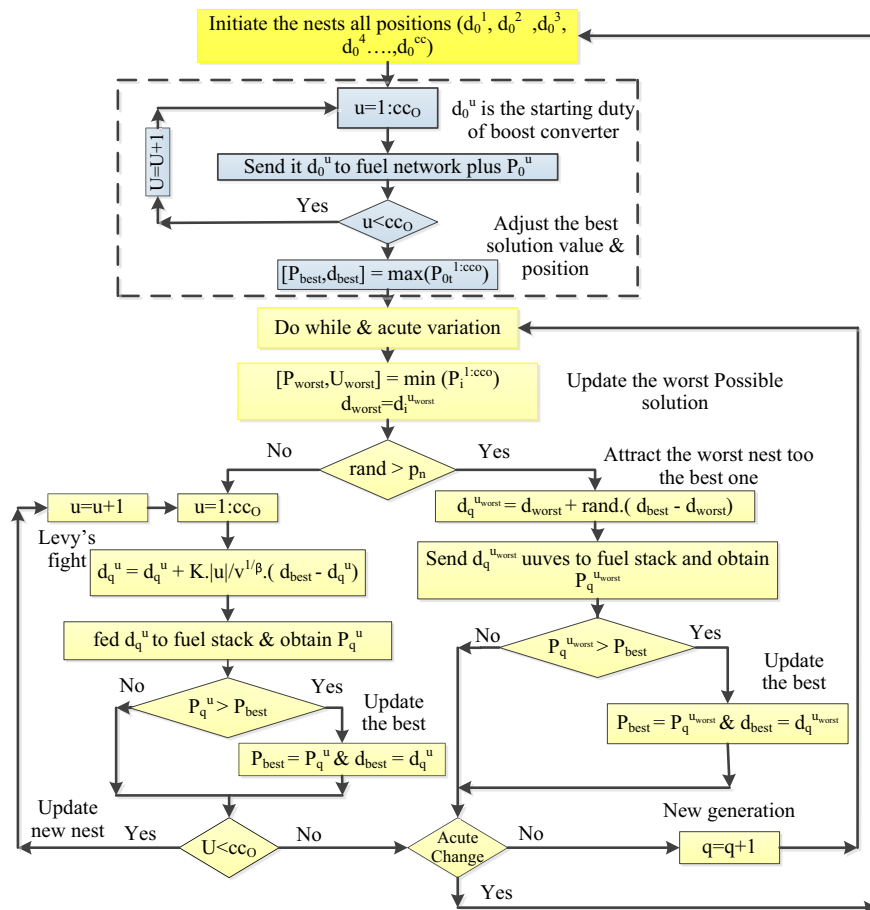


**Figure 8.** Adjustable Levy value-based cuckoo search power point identifier for PEMFS.

the multiple dimensional oriented complex problems. The limitations of these conventional technologies are compensated by selecting the modified PSO-dependent ANFIS controller. In this proposed concept, the ANFIS-related membership functions, and their utilized constants are finalized by applying the swarm intelligence methodology. The working structure of this introduced hybrid methodology is mentioned in Fig. 9. From Fig. 9, and Eq. (16), the starting functioning of the hybrid controller, an adaptive swarm intelligence utilizes the very low level of agents for searching the local fuel stack optima. After that, the swarm concept selects and applies the

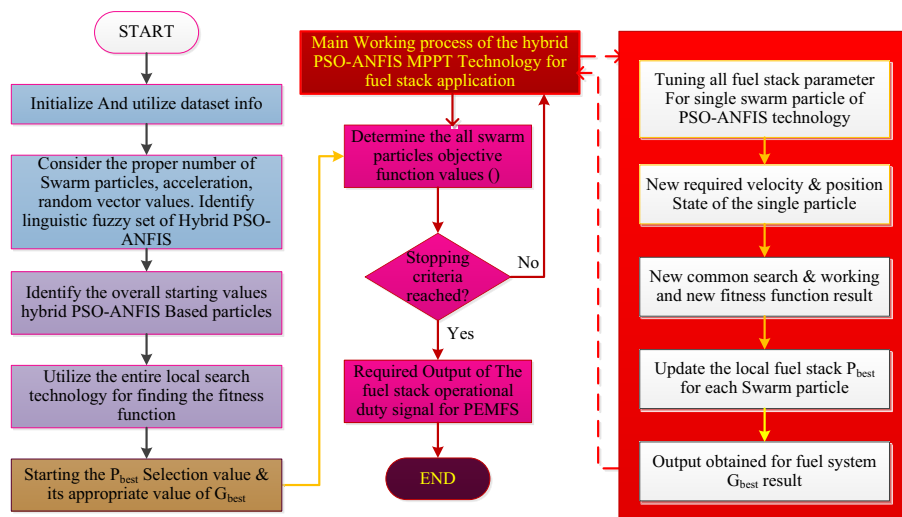


**Figure 9.** Introduced hybrid swarm intelligence dependent ANFIS power point identifier for PEMFS.

appropriate membership functions to the ANFIS block to give the accurate MPP place of the proposed power production network.

$$\text{if } R \text{ is } F_1 \ \& \ T \text{ is } G_1 \text{ then } V = J_1s + K_1n + r_1 \tag{16}$$

$$\text{if } R \text{ is } F_2 \ \& \ T \text{ is } G_2 \text{ then } V = J_2s + K_2n + r_2 \tag{17}$$

$$Q_{1,c} = \mu_{R1}(s) + \mu_{T1}(n); \ c = 1, 2 \tag{18}$$

$$Q_{2,c} = \mu_{R2}(s) + \mu_{T2}(n); \ c = 1, 2 \tag{19}$$

where the parameters R, T, F, and G are the ANFIS network membership functions and their source signals. From Fig. 9, the J, K, and r are the utilized subsequent parameters.

### Development of wide voltage supply DC–DC circuit

The power conversion of the renewable power network is completely depending on the power transmission of the DC–DC circuit. Also, the utilized fuel stack network utilization factor depends on the power converter circuit. There are several power DC–DC circuit models have existed in the literature for most renewable power strategy systems. In this work, a new less passive component involved in wide power transmission circuit topology is introduced for improving the hydrogen-based fuel stack voltage. This converter circuit is interfaced with one power switch (S), five power diode switches ( $D_x, D_y, D_z, D_s, D_g$ ), dual passive electromagnetic energy stored inductors ( $L_a, L_b$ ), and five capacitive elements ( $C_x, C_y, C_z, C_s$ , and  $C_g$ ). The inductive electromagnetic components charged, average, plus discharged currents and voltages are  $I_{La-cgs}, I_{Lb-cgs}, I_{La}, I_{Lb}, I_{La-dcgs}, I_{Lb-dcgs}, V_{La-cgs}, V_{Lb-cgs}, V_{La}, V_{Lb}, V_{La-dcgs}$ , and  $V_{Lb-dcgs}$  respectively. Similarly, the capacitive oriented charged, average, and discharged voltages plus currents are  $V_{Cx-cgs}, V_{Cy-cgs}, V_{Cz-cgs}, V_{Cs-cgs}, V_{Cg-cgs}, V_{Cx}, V_{Cy}, V_{Cz}, V_{Cs}, V_{Cg}, V_{Cx-dcgs}, V_{Cy-dcgs}, V_{Cz-dcgs}, V_{Cs-dcgs}, V_{Cg-dcgs}, I_{Cx-cgs}, I_{Cy-cgs}, I_{Cz-cgs}, I_{Cs-cgs}, I_{Cg-cgs}, I_{Cx}, I_{Cy}, I_{Cz}, I_{Cs}, I_{Cg}, I_{Cx-dcgs}, I_{Cy-dcgs}, I_{Cz-dcgs}, I_{Cs-dcgs}$ , and  $I_{Cg-dcgs}$  respectively.

### Operating state analysis of DC–DC power converter

From Fig. 10a, the wide power DC–DC circuit utilized switch (s) moves in the working state of the fuel stack-based energy supply system. The applied voltage and switch currents of the considered switch are  $V_s$ , and  $I_s$ . In this switching functioning, the utilized diodes  $D_x$ , and  $D_s$  come under the utilization state and the remaining three diodes  $D_y, D_z,$  and  $D_g$  go into the blocking state. Here, all the five diodes voltages under functioning and nonfunctioning stages are evaluated as  $V_{Dxon}, V_{Dyoff}, V_{Dzoff}, V_{Dson}, V_{Dgoff}, V_{Dsoff}, V_{Dyon}, V_{Dzon}, V_{Dsoff}$  and  $V_{Dgon}$ . Similarly, the switch on plus off stage currents plus voltages is evaluated as  $I_{Son}, I_{Soff}, V_{Son}, V_{Soff}$  respectively. The switching on state voltages is mentioned in Eq. (20). After time  $DT_s$ , the MOSFET movement starts goes in blocking stage of the system then the inductors charging on state voltages, and their stage voltages are represented

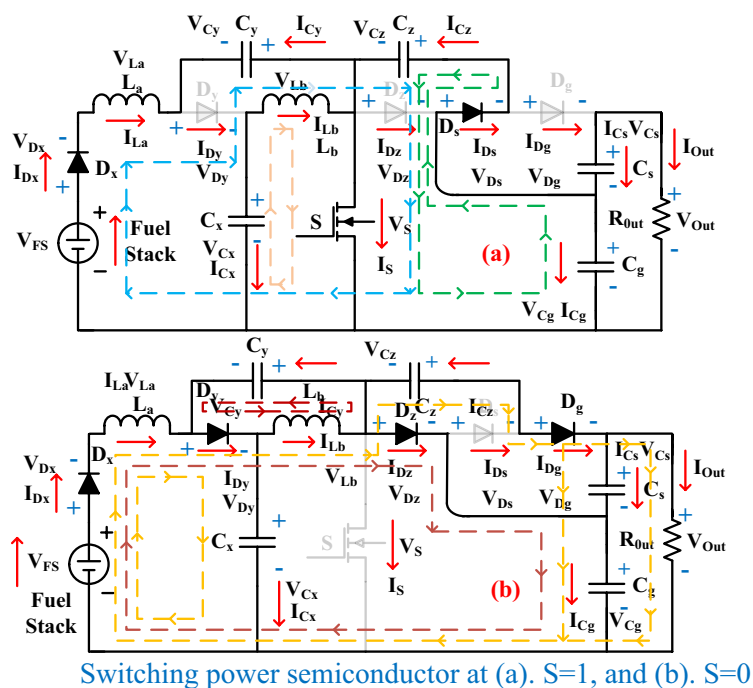


**Figure 10.** Switching power semiconductor at (a)  $S=1$ , and (b)  $S=0$ . (c) Proposed new DC–DC circuit operational waveforms.

as  $V_{Laon}$ ,  $V_{Lbon}$ ,  $V_{Laoff}$  and  $V_{Lboff}$  respectively. The capacitors utilized voltages at the blocking stage of the system are mentioned in Eq. (21), and its corresponding circuit is given in Fig. 10b.

$$\begin{cases} V_{Laon} = V_{FS} + V_{Cy} \\ V_{Lbon} = V_{Cx} \\ V_{Cz} = V_{Cg} \\ V_{Out} = V_{Cs} + V_{Cg} \end{cases} \quad (20)$$

$$\begin{cases} V_{Laoff} = V_{FS} - V_{Cx} \\ V_{Laoff} = V_{FS} - V_O + V_{Cy} + V_{Cz} \\ V_{Lboff} = -V_{Cy} \\ V_{Cz} = V_{Cs} \end{cases} \quad (21)$$

$$\begin{cases} V_{Laon} * Td + V_{Laoff} * T(1 - d) = 0 \\ V_{Lboff} * dT + V_{Lbon} * T(1 - d) = 0 \end{cases} \quad (22)$$

$$\begin{cases} V_{Cx} = \frac{1-d}{1-2d} V_{FS} \\ V_{Cy} = \frac{d}{1-2d} V_{FS} \\ V_{Cz} = V_{Cs} = V_{Cg} = V_{Out}/2 \\ V_{Out} = \frac{2d}{1-2d} V_{FS} \end{cases} \quad (23)$$

$$M = \frac{V_{FS}}{V_{Out}} = \frac{2}{1 - 2d} \quad (24)$$

### Voltage and current stress analysis of switching devices

The appeared voltages of all semiconductor switches under various conduction durations are mentioned in Fig. 10c. From Fig. 10c, all the diode's conduction and ideal stages of the voltages are equal to half of the utilized load voltages. Here, the load voltages are completely controlled by capacitor  $C_g$  and it manages the uniform restive voltage under various disturbances that occur across the switches. The current that appeared across the diodes and switch is mentioned in Eq. (27). From Eq. (31), it has been identified that the average currents of inductors are similar and it is equal to the fraction of the load current. The capacitive charged voltages are mentioned in Eqs. (32) to (36).

$$\begin{cases} V_{Cx} = \frac{1-d}{2} V_{Out} \\ V_{Cy} = \frac{d}{2} U_O \\ V_{Cz} = V_{Cs} = V_{Cg} = V_{Out}/2 \end{cases} \quad (25)$$

$$V_{Cg} = V_{Cx} + V_{Cy} \quad (26)$$

$$\begin{cases} I_{Cxon} = -I_{Lb} \\ I_{Cyon} = -I_{La} \\ I_{Cson} = -I_{out} \\ I_{Cgon} = -(-I_{Cson} + I_{Czon}) \end{cases} \quad (27)$$

$$\begin{cases} I_{Cxoff} = I_{Cyoff} + I_{La} - I_{Lb} \\ I_{Czoff} = -I_{Csoff} - I_{Load} \\ I_{Cgoff} = I_{La} - I_{Load} - I_{Cxoff} \end{cases} \quad (28)$$

$$\begin{cases} I_{Cxon} \times dT + I_{Cxoff} \times (1 - d)T = 0 \\ I_{Cyon} \times dT + I_{Cyoff} \times (1 - d)T = 0 \\ I_{Czon} \times dT + I_{Czoff} \times (1 - d)T = 0 \\ I_{Cson} \times dT + I_{Csoff} \times (1 - d)T = 0 \\ I_{Cgon} \times dT + I_{Cgoff} \times (1 - d)T = 0 \end{cases} \quad (29)$$

$$I_{FS} = \frac{2}{1 - 2d} I_{out} \quad (30)$$

$$I_{La} = I_{Lb} = I_{in} = \frac{2}{1 - 2d} I_{out} \quad (31)$$

$$\begin{cases} I_{Cxon} = -\frac{2I_{out}}{1-2d} \\ I_{Cxoff} = \frac{2dI_{out}}{(1-2d)(1-d)} \end{cases} \quad (32)$$

$$\begin{cases} I_{Cyon} = -\frac{2I_{out}}{1-2d} \\ I_{Cyoff} = \frac{2dI_{out}}{(1-2d)(1-d)} \end{cases} \quad (33)$$

$$\begin{cases} I_{Czon} = \frac{1}{d}I_{out} \\ I_{Czoff} = \frac{-1}{1-d}I_{out} \end{cases} \quad (34)$$

$$\begin{cases} I_{Cson} = -I_{out} \\ I_{Csoff} = \frac{d}{1-d}I_{out} \end{cases} \quad (35)$$

$$\begin{cases} I_{Cgon} = -\frac{d+1}{d}I_{out} \\ I_{Cgoff} = \frac{1+d}{1-d}I_{out} \end{cases} \quad (36)$$

$$I_S = I_{La} + I_{Lb} + I_{Czon} = \frac{1+2d}{d(1-2d)}I_{out} \quad (37)$$

$$I_{Ds} = -I_{Cgon} = \frac{d+1}{d}I_{out} \quad (38)$$

$$I_{Dy} = I_{Cyoff} + I_{La} = \frac{2}{(1-2d)(1-d)}I_{out} \quad (39)$$

$$I_{Dz} = I_{Lb} - I_{Cyoff} - (-I_{Czoff}) = \frac{1}{1-d}I_{out} \quad (40)$$

$$I_{Dg} = -I_{Czoff} = \frac{1}{1-d}I_{out} \quad (41)$$

### Design of capacitive and inductive components

In every power transmission circuit, the design of inductive elements plays a main role in the utilized system. Here, the voltage distribution law is applied to identify the static potential variation of all the capacitive and inductive components. The selected source inductor value should be more to satisfy the uniform voltage supply to the fuel stack and its derivation is mentioned in Eq. (42). Similarly, the capacitive elements are utilized based on the operational system frequency which is given in Eq. (43).

$$\begin{cases} L_b = v_L \frac{dt}{d_{i,b}} \\ I_a = L_b = \frac{d(1-d)V_{FS}}{(1-2d)\Delta I_f} \end{cases} \quad (42)$$

$$\begin{cases} C_x = \frac{2dI_{out}}{(1-2d)\Delta V_{Cx}f} \\ C_y = \frac{2d^2I_{out}}{(1-2d)\Delta V_{Cy}f} \\ C_z = \frac{2I_{out}}{\Delta V_{Cz}f} \\ C_s = \frac{4dI_{out}}{(1-2d)^2\Delta V_{Cs}f} \\ C_g = \frac{(1+d)I_{out}}{\Delta V_{Cg}f} \end{cases} \quad (43)$$

### Proposed system simulation results

The proposed polymer membrane depending wide power supply converter network is implanted by utilizing the MATLAB/Simulink tool. The derived source capacitor  $C_x$  value is equal to  $280\mu\text{F}$  and it helps the fuel energy production system from various hydrogen chemical reactions and water membrane content. The elements  $C_y$ ,  $C_z$ ,  $C_s$ ,  $L_b$ ,  $D_y$ ,  $D_z$ , and  $D_s$  function as an electric filter circuit for optimizing the fuel stack voltage disturbances and enhancing the voltage transformation value of the source network. Also, this  $LC^3D^2$  circuit reduces the voltage levels that appear near the power diodes and switching elements. The utilized 3 capacitors  $C_y$ ,  $C_z$ ,  $C_s$  values are  $120\mu\text{F}$ ,  $225\mu\text{F}$ , and  $225\mu\text{F}$  respectively. The capacitor  $C_g$  is placed near parallel to the load resistive element ( $R_{out}$ ) for handling the standalone network dc-bus voltages and its related value is  $180\mu\text{F}$ . Finally, the selected resistive component value is  $68\Omega$ . The inductive elements  $L_a$  and  $L_b$  values are equal to  $100\text{mH}$  respectively. Here, the

suitable inductive values provide constant dc-bus voltage, and its internal resistive property is taken as zero for achieving the grid unity power factor.

### Analysis of universal source power-fed polymer membrane cell at 298 K

The polymer stack fuel device source current is very excessive. Due to this excessive supply current of the polymer fuel stack, the direct voltage feeding to the telecommunication system is quite risky work. Also, the polymer fuel stack device depending on power transfer circuit production current, converter source terminal voltages, and its associated total power generation are mentioned in Fig. 11a–f, respectively. From Fig. 11, the polymer fuel device and unique switch production currents, available voltages, and produced powers by applying the AVSV-P&O, ASB-FLC, MSL-PSO, ALV-CSO, and MPSO-ANFIS power point identifiers are 21.003 A, 23.7745 V, 498.5523 W, 2.8459 A, 167.760 V, 482.648 W, 20.917 A, 23.897 V, 499.978 W, 2.87765 A, 166.080 V, 484.124 W, 20.941 A, 23.913 V, 500.7721 W, 2.9894 A, 162.494 V, 485.697 W, 20.872 A, 23.997 V, 500.881 W, 2.9945 A, 165.408 V, 486.300 W, 20.813 A, 24.0712 V, 500.993 W, 3.0929 A, 157.409 V, and 486.711 W respectively.

From Fig. 11c, the fuel stack-based modified swarm intelligence-dependent ANFIS technology takes very low-level tracing time and provides the maximum possible efficiency are 0.0299 s, and 97.1564% respectively. Similarly, the fuzzy, cuckoo and conventional swarm controllers' energy production capability is low level when equated to the ANFIS hybrid methodology and these methodologies give the functioning point identifying time,

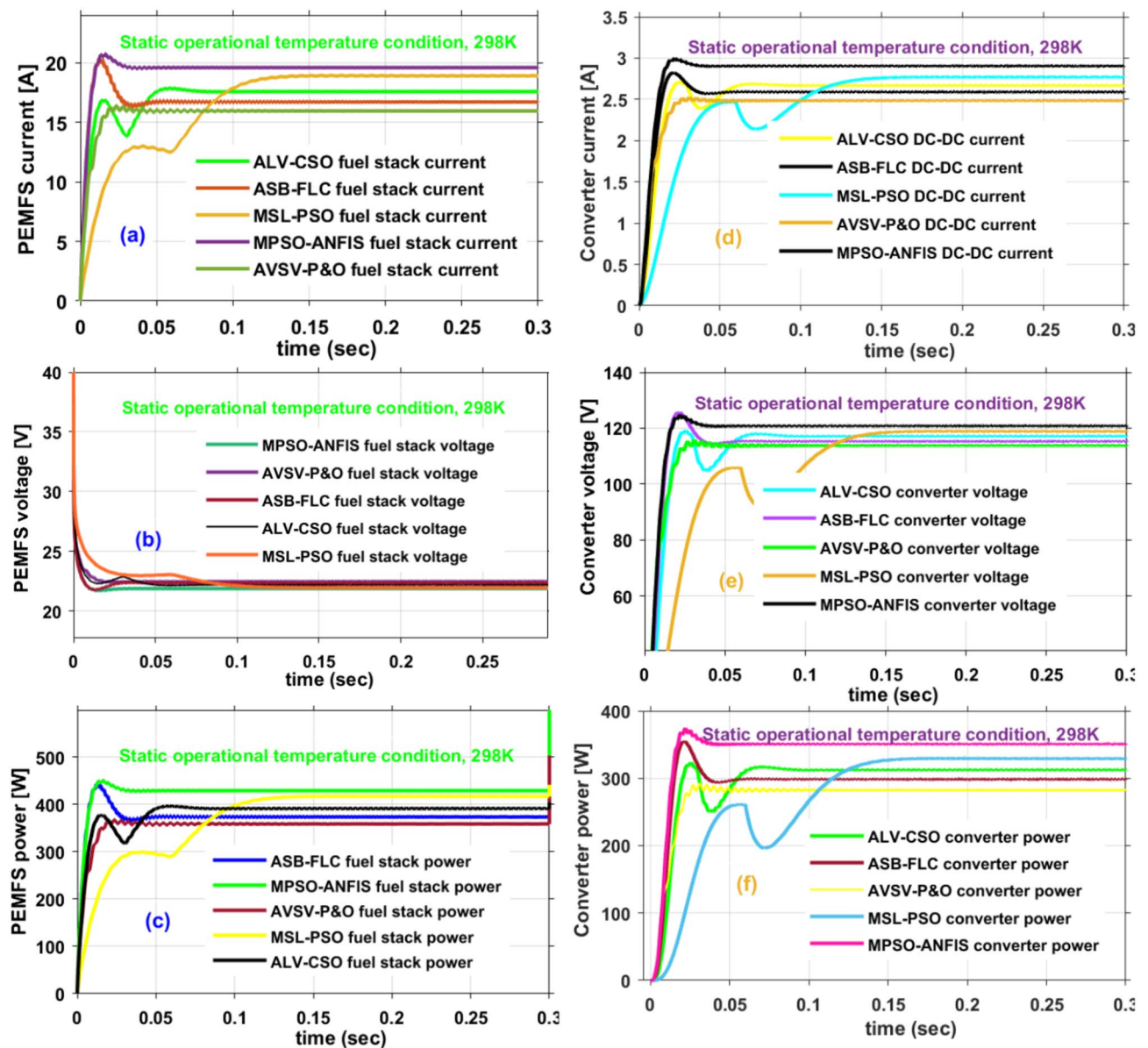


**Figure 11.** (a) Polymer membrane cell current, (b) polymer membrane cell voltage, (c) polymer membrane cell power, (d) DC-DC circuit current, (e) DC-DC circuit voltage, (f) DC-DC circuit power at uniform temperature value 298 K.



and its power transferring efficiency values are 0.0321 s, 96.854%, 0.0307 s, 97.0923%, 0.0317 s, and 96.9932%. So, the fuzzy is unable to provide the peak power position of the polymer-based fuel device with more efficiency. Also, the particle swarm and cuckoos-related technologies help the proposed new DC–DC converter to operate in uniform current supply mode. From Fig. 11d and e, the advanced variable step value-based perturb & observe (AVSV-P&O), and Adaptive step-based Fuzzy Logic Controller development takes very low-level time and it takes less amount for installation and maintenance.

### Analysis of universal DC–DC circuit-fed polymer cell at 298 K, 341 K, and 370 K

The polymer-depending fuel device integrated interleaved power DC–DC network production current quantity, voltage source, and powers are defined in Fig. 12a–f. The AVSV-P&O and ASB-FLC-based controllers have not generated the complete uniform polymer fuel stack device production current. Also, these methodologies capture the low-level voltage of the system and take a high amount of convergence time to catch the functioning peak voltage of the proposed fuel stack network. However, the AVSV-P&O, ASB-FLC, MSL-PSO, ALV-CSO, and MPSO-ANFIS fed polymer fuel device and introduced new DC–DC circuit supply currents, utilized voltages, and their produced peak powers and efficiencies at 341 K are 25.709 A, 32.4478 V, 834.0051 W, 3.9981 A, 204.144 V, 816.171 W, 97.4532%, 25.690 A, 32.578 V, 836.9167 W, 4.1827 A, 195.882 V, 819.181 W, 25.619 A, 32.669 V,

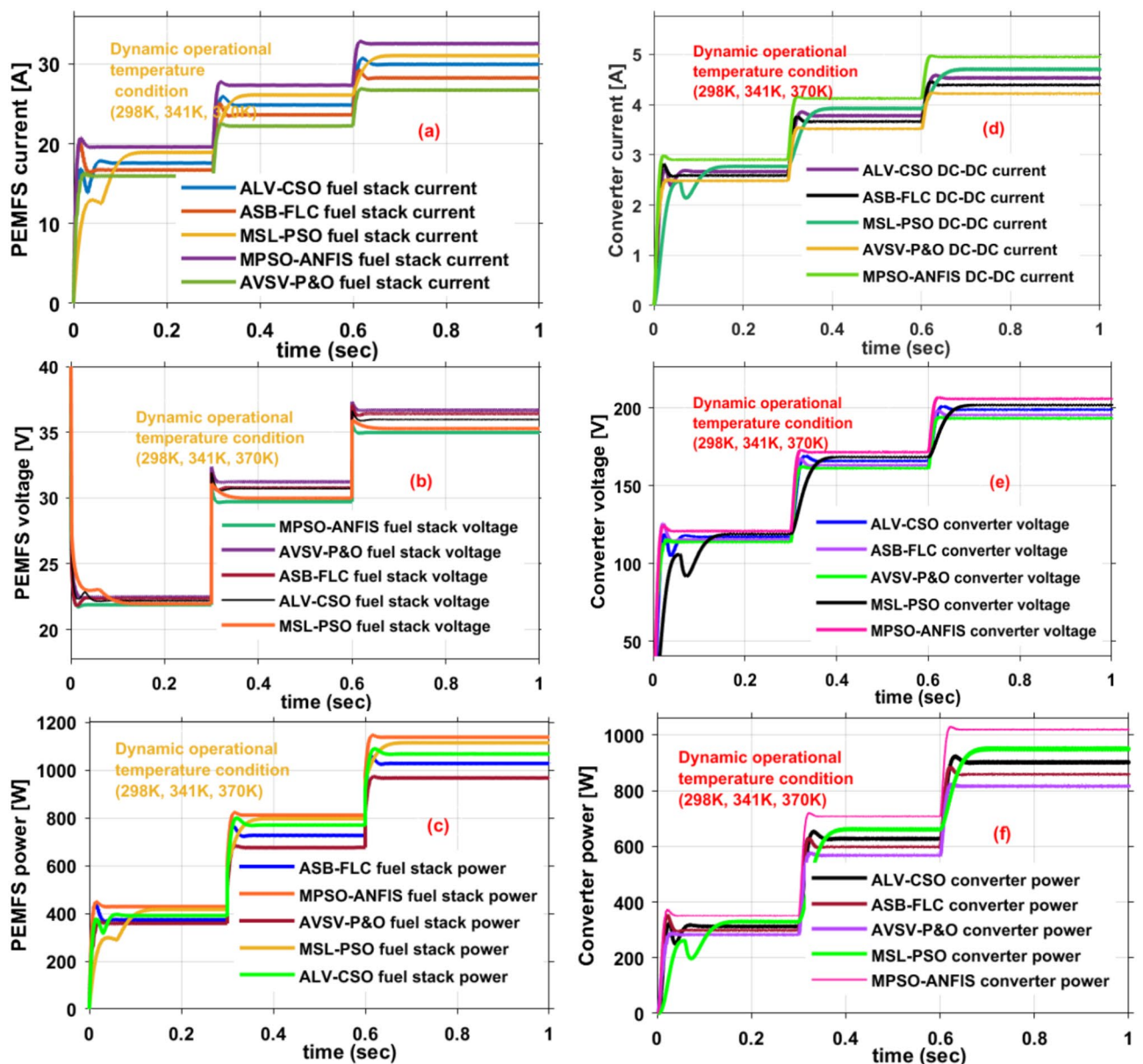


**Figure 12.** (a) Polymer membrane cell current, (b) polymer membrane cell voltage, (c) polymer membrane cell power, (d) DC–DC circuit current, (e) DC–DC circuit voltage, (f) DC–DC circuit power at various temperature values 298 K, 341 K, and 370 K.



MPPT Category	Current of cell (A)	Voltage of cell (V)	Power of cell (W)	DC–DC current (A)	DC–DC voltage (V)	DC–DC power (W)	Efficiency (%)	MPP trace time (sec)	Disturbance in MPP
AVSV-P&O	31.382	34.573	1080.973	5.0856	207.472	1057.90	97.8432	0.022892	Heavy
ASB-FLC	30.670	35.889	1100.737	5.1882	206.504	1071.34	97.9923	0.02123	Heavy
MSL-PSO	31.219	35.991	1123.619	5.1997	212.696	1105.80	98.4169	0.192	Moderate
ALV-CSO	30.763	36.544	1124.228	5.2136	212.941	1110.06	98.7431	0.0188	Moderate
MPSO-ANFIS	30.549	36.985	1129.887	5.22412	218.872	1143.39	98.819	0.0151	Low level
AVSV-P&O	25.709	32.4478	834.0051	3.9981	204.144	816.171	97.4532	0.030132	Heavy
ASB-FLC	25.690	32.578	836.9167	4.1827	195.882	819.181	97.8776	0.02657	Heavy
MSL-PSO	25.619	32.669	836.9786	4.42956	185.025	819.477	97.9109	0.02591	Moderate
ALV-CSO	25.564	32.7416	837.098	4.4473	185.562	820.186	97.9923	0.0253	Moderate
MPSO-ANFIS	25.429	32.992	838.973	4.4918	183.205	822.777	98.0785	0.0202	Low level
AVSV-P&O	21.003	23.7745	498.5523	2.8459	167.760	482.648	96.8178	0.0347	Heavy
ASB-FLC	20.917	23.897	499.978	2.87765	166.080	484.124	96.854	0.0321	Heavy
MSL-PSO	20.941	23.913	500.7721	2.9894	162.494	485.697	96.9932	0.0317	Moderate
ALV-CSO	20.872	23.997	500.881	2.9945	165.408	486.300	97.0923	0.0307	Moderate
MPSO-ANFIS	20.813	24.0712	500.993	3.0929	157.409	486.711	97.1564	0.0299	Low level

**Table 2.** Identified polymer membrane-based fuel network fed wide power transmission converter circuit at multiple temperature values.

836.9786 W, 4.42956 A, 185.025 V, 819.477 W, 97.9109%, 25.564 A, 32.7416 V, 837.098 W, 4.4473 A, 185.562 V, 820.186 W, 97.9923%, 25.429 A, 32.992 V, 838.973 W, 4.4918 A, 183.205 V, 822.777 W, and 98.0785% efficiency.

From Fig. 12d, the fuzzy, swarm, and cuckoo methodologies tracing time of the peak current of the fuel stack polymer membrane system at 341 K are 0.02657 s, 0.02591 s, and 0.0253 s respectively. So, the introduced ANFIS hybrid network utilizes a very low level settling time of the DC–DC load power thereby supplying the potential energy to the electrical vehicle system with more efficiency. Here, the nature-dependent swarm methodologies design takes medium complexity when equated with the hybridization concepts. At 370 K functioning system temperature, the overall polymer membrane device, and wide energy supply DC–DC converter currents, utilized voltage values, and their corresponding powers by integrating the AVSV-P&O, ASB-FLC, MSL-PSO, ALV-CSO, and MPSO-ANFIS blocks are 31.382 A, 34.573 V, 1080.973 W, 5.0856 A, 207.472 V, 1057.90 W, 30.670 A, 35.889 V, 1100.737 W, 5.1882 A, 206.504 V, 1071.34 W, 31.219 A, 35.991 V, 1123.619 W, 5.1997 A, 212.696 V, 1105.80 W, 30.763 A, 36.544 V, 1124.228 W, 5.2136 A, 212.941 V, 1110.06 W, 30.549 A, 36.985 V, 1129.887 W, 5.22412 A, 218.872 V, and 1143.39 W respectively. The detailed investigation of the polymer-based fuel network and its interconnected DC–DC voltage transmission circuit power values at multiple operational temperature value conditions are mentioned in Table 2.

### Ethical approval

This paper does not contain any studies with human participants or animals performed by any of the authors.

### Conclusion

The polymer material-based fuel module network interfaced more voltage conversion ratio DC–DC circuit is studied by following the MATLAB tool. In the 1st objective, the fuel stack is developed by selecting the polymer membrane because it provides quick network response, more energy density, low warm-up time, fewer wear issues, and more applicable stationary networks. However, this fuel device faces the challenges are low amount of voltage supply and low fuel cell durability. So, the new power conversion circuit is developed to improve the fuel stack potential supply. These DC–DC circuit features are good potential transformation efficiency, low level of voltage values appearing across the silicon diodes, less passive elements usage, better system static behavior, and capability to work for any renewable energy networks. Here, the duty signal, and MPP point are identified by developing the modified swarm controller-dependent ANFIS network is implemented. From the simulation results investigation of the proposed system, the ANFIS hybrid block provides good power points identifying accuracy, is easy to implement, low-level iterations are utilized, better dynamic behavior, and low-level dependence on the system development.

### Data availability

The datasets used and/or analyzed during the current study are available from the corresponding author upon reasonable request.

Received: 2 July 2024; Accepted: 8 August 2024

Published online: 13 August 2024

## References

1. Reis, A. L. *et al.* A review of operational control strategies in water supply systems for energy and cost efficiency. *Renew. Sustain. Energy Rev.* **175**, 113140. <https://doi.org/10.1016/j.rser.2022.113140> (2023).
2. Ali, H. M. *et al.* Advances in thermal energy storage: Fundamentals and applications. *Progr. Energy Combust. Sci.* **100**, 101109 (2024).
3. Fa-qiang, S. *et al.* Estimation of the cavity volume in the gasification zone for underground coal gasification under different oxygen flow conditions. *Energy* **285**, 129309 (2023).
4. Shahzad, U. *et al.* The role of biomass energy consumption and economic complexity on environmental sustainability in G7 economies. *Bus. Strat. Environ.* **32**(1), 781–801. <https://doi.org/10.1002/bse.3175> (2023).
5. Hussaian Basha, C. H. & Rani, C. Different conventional and soft computing MPPT techniques for solar PV systems with high step-up boost converters: A comprehensive analysis. *Energies* **13**(2), 371 (2020).
6. Hashemzadeh, S. M. *et al.* Design and modelling of a new three winding coupled inductor based high step-up DC–DC converter for renewable energy applications. *IET Power Electron.* **15**(13), 1322–1339 (2022).
7. Khan, M. Y. A. *et al.* A novel high step-up DC–DC converter with improved P&O MPPT for photovoltaic applications. *Electric Power Compon. Syst.* **49**(9), 884–900 (2021).
8. Feng, Ye., Chen, J. & Luo, Ji. Life cycle cost analysis of power generation from underground coal gasification with carbon capture and storage (CCS) to measure the economic feasibility. *Resour. Policy* **92**, 104996 (2024).
9. Li, B. *et al.* The future of Green energy: A panel study on the role of renewable resources in the transition to a Green economy. *Energy Econ.* **127**, 107026. <https://doi.org/10.1016/j.eneco.2023.107026> (2023).
10. Li, S. *et al.* A fast and accurate calculation method of line breaking power flow based on Taylor expansion. *Front. Energy Res.* **10**, 943946 (2022).
11. Shayeghi, H. *et al.* Presenting of the magnetic coupling-based transformer-less High Step-Up DC–DC converter for renewable energy applications. *Int. Trans. Electr. Energy Syst.* **2022**, 1–15. <https://doi.org/10.1155/2022/3141119> (2022).
12. Wang, H. *et al.* A MTPA and flux-weakening curve identification method based on physics-informed network without calibration. *IEEE Transactions on Power Electronics* **38**(10), 12370–12375. <https://doi.org/10.1109/TPEL.2023.3295913> (2023).
13. Shi, Y. *et al.* RayMVSNet++: Learning ray-based 1D implicit fields for accurate multi-view stereo. *IEEE Trans. Pattern Anal. Mach. Intell.* <https://doi.org/10.1109/TPAMI.2023.3296163> (2023).
14. Hussaian Basha, C. H. & Rani, C. Performance analysis of MPPT techniques for dynamic irradiation condition of solar PV. *Int. J. Fuzzy Syst.* **22**(8), 2577–2598 (2020).
15. Jiang, W., Ren, T. & Qianhua, Fu. Deep learning in the phase extraction of electronic speckle pattern interferometry. *Electronics* **13**(2), 418 (2024).
16. Zhang, R. *et al.* Centralized active power decoupling method for the CHB converter with reduced components and simplified control. *IEEE Trans. Power Electron.* **39**(1), 47–52. <https://doi.org/10.1109/TPEL.2023.3321671> (2024).
17. Li, P. *et al.* A distributed economic dispatch strategy for power–water networks. *IEEE Trans. Control Netw. Syst.* **9**(1), 356–366 (2021).
18. Duan, Y., Zhao, Y. & Jiangping, Hu. An initialization-free distributed algorithm for dynamic economic dispatch problems in microgrid: Modeling, optimization and analysis. *Sustain. Energy Grids Netw.* **34**, 101004 (2023).
19. Shirkhani, M. *et al.* A review on microgrid decentralized energy/voltage control structures and methods. *Energy Rep.* **10**, 368–380. <https://doi.org/10.1016/j.egyrs.2023.06.022> (2023).
20. Nadimuthu, L. P. R. *et al.* Energy conservation approach for continuous power quality improvement: A case study. *IEEE Access* **9**, 146959–146969 (2021).
21. Meng, Q. *et al.* An online reinforcement learning-based energy management strategy for microgrids with centralized control. *IEEE Trans. Ind. Appl.* <https://doi.org/10.1109/TIA.2024.3430264> (2024).
22. Udhay Sankar, V. *et al.* Application of WDO for decision-making in combined economic and emission dispatch problem. In *SocProS 2018 Vol. 1* (eds Das, K. N. *et al.*) (Springer, 2020).
23. Zhang, J. *et al.* A novel multiport transformer-less unified power flow controller. *IEEE Trans. Power Electron.* **39**(4), 4278–4290. <https://doi.org/10.1109/TPEL.2023.3347900> (2024).
24. Zhang, J. *et al.* An embedded DC power flow controller based on full-bridge modular multilevel converter. *IEEE Trans. Ind. Electron.* **71**(3), 2556–2566. <https://doi.org/10.1109/TIE.2023.3265041> (2024).
25. Wang, S. *et al.* An identification method for anomaly types of active distribution network based on data mining. *IEEE Trans. Power Syst.* <https://doi.org/10.1109/TPWRS.2023.3288043> (2023).
26. Liu, Q. *et al.* Transfer-free in-situ synthesis of high-performance polybenzimidazole grafted graphene oxide-based proton exchange membrane for high-temperature proton exchange membrane fuel cells. *J. Power Sour.* **559**, 232666. <https://doi.org/10.1016/j.jpowsour.2023.232666> (2023).
27. Zhao, H. *et al.* Realizing dendrite-free lithium deposition with three-dimensional soft-rigid nanofiber interlayers. *J. Colloid Interface Sci.* **666**, 131–140. <https://doi.org/10.1016/j.jcis.2024.04.029> (2024).
28. Yuntao, J. *et al.* Distributed three-phase power flow for AC/DC hybrid networked microgrids considering converter limiting constraints. *IEEE Trans. Smart Grid* **13**(3), 1691–1708. <https://doi.org/10.1109/TSG.2022.3140212> (2022).
29. Zhang, H. *et al.* High-dynamic and low-cost sensorless control method of high-speed brushless DC motor. *IEEE Trans. Ind. Inform.* **19**(4), 5576–5584. <https://doi.org/10.1109/TII.2022.3196358> (2023).
30. Hashemzadeh, S. M. *et al.* (2022) "Design and analysis of a new coupled inductor-based interleaved high step-up DC–DC converter for renewable energy applications. *Int. Trans. Electr. Energy Syst.* **1**, 7618242 (2022).
31. Ramakrishna Reddy, K., Hussaian Basha, C. H. & Prashanth, V. A novel on energy management strategy with maximum exploitation of renewables and EV storage in distribution networks. *Int. Trans. Electr. Energy Syst.* **2023**, 1–18. <https://doi.org/10.1155/2023/1365608> (2023).
32. Hussaian Basha, C. H. & Rani, C. Application of fuzzy controller for two-leg inverter solar PV Grid connected systems with high voltage gain boost converter. *J. Eng. Sci. Technol. Rev.* **14**(2), 8–17. <https://doi.org/10.25103/jestr.142.02> (2021).
33. Song, F., Liu, Y., Shen, D., Li, L. & Tan, J. Learning control for motion coordination in wafer scanners: toward gain adaptation. *IEEE Trans. Ind. Electron.* **69**(12), 13428–13438. <https://doi.org/10.1109/TIE.2022.3142428> (2022).
34. Song, F., Liu, Y., Dong, Y., Chen, X. & Tan, J. Motion control of wafer scanners in lithography systems: From setpoint generation to multi-stage coordination. *IEEE Trans. Instrum. Meas.* <https://doi.org/10.1109/TIM.2024.3413202> (2024).
35. Hashemzadeh, S. M. & Hejri, M. A fast and accurate global maximum power point tracking method for solar strings under partial shading conditions. *J. Op. Autom. Power Eng.* **8**(3), 245–256 (2020).
36. Hussaian Basha, C. H. *et al.* "Design and performance analysis of common duty ratio controlled zeta converter with an adaptive P&O MPPT controller. In *Proceedings of International Conference on Data Science and Applications: ICDSA 2021 Vol. 1* (eds Saraswat, M. *et al.*) (Springer, 2022).
37. Mariprasath, T. *et al.* Design and analysis of an improved artificial neural network controller for the energy efficiency enhancement of wind power plant. In *Computational Methods and Data Engineering: Proceedings of ICCMDE 2021* (eds Asari, V. K. *et al.*) 67–77 (Springer, 2022).

38. Pathak, P. K. *et al.* Modified incremental conductance MPPT algorithm for SPV-based grid-tied and stand-alone systems. *IET Gener. Trans. Distrib.* **16**(4), 776–791 (2022).
39. Ballaji, A. *et al.* Design & development of MPPT using PSO with predefined search space based on fuzzy fokker planck solution. *IEEE Access* **10**, 80764–80783 (2022).
40. Bisht, R. & Sikander, A. An improved method based on fuzzy logic with beta parameter for PV MPPT system. *Optik* **259**, 168939 (2022).
41. Aly, M. & Rezk, H. An improved fuzzy logic control-based MPPT method to enhance the performance of PEM fuel cell system. *Neural Comput. Appl.* **34**, 4555–4566 (2022).
42. Sarvi, M. & Azadian, A. A comprehensive review and classified comparison of MPPT algorithms in PV systems. *Energy Syst.* **13**(2), 281–320 (2022).
43. Nga Thi-Thuy, V., Nguyen, H. D. & Nguyen, A. T. Reinforcement learning-based adaptive optimal fuzzy MPPT control for variable speed wind turbine. *IEEE Access* **10**, 95771–95780 (2022).
44. Basha, C. H. & Murali, M. A new design of transformerless, non-isolated, high step-up DC-DC converter with hybrid fuzzy logic MPPT controller. *Int. J. Circuit Theory Appl.* **50**(1), 272–297. <https://doi.org/10.1002/cta.3153> (2022).
45. Kumbhar, A. *et al.* Reducing grid dependency and operating cost of micro grids with effective coordination of renewable and electric vehicle's storage. In *Soft Computing for Problem Solving: Proceedings of the SocProS2* (eds Thakur, M. *et al.*) 639–653 (Springer, 2023).
46. Hussaian Basha, C. H., Viraj Bansal, C., Rani, R. M. & Brisilla, S. O. Development of cuckoo search MPPT algorithm for partially shaded solar PV SEPIC converter. In *Soft Computing for Problem Solving: SocProS 2018 Vol. 1* (eds Das, K. N. *et al.*) 727–736 (Springer, 2020). [https://doi.org/10.1007/978-981-15-0035-0\\_59](https://doi.org/10.1007/978-981-15-0035-0_59).

## Acknowledgements

We would like to thank SR University, Hanumakonda 506371, Telangana, India management for supporting us in carrying out this work. Also, this work was supported by the Researchers Supporting Project number (RSPD2024R646), King Saud University, Riyadh, Saudi Arabia.

## Author contributions

All authors contributed to the study, conception, and design. all authors commented on the manuscript. All authors read and approved the final manuscript.

## Funding

The authors did not receive support from any organization for the submitted work.

## Competing interests

The authors declare no competing interests.

## Additional information

**Correspondence** and requests for materials should be addressed to C.H.H.B.

**Reprints and permissions information** is available at [www.nature.com/reprints](http://www.nature.com/reprints).

**Publisher's note** Springer Nature remains neutral with regard to jurisdictional claims in published maps and institutional affiliations.

**Open Access** This article is licensed under a Creative Commons Attribution-NonCommercial-NoDerivatives 4.0 International License, which permits any non-commercial use, sharing, distribution and reproduction in any medium or format, as long as you give appropriate credit to the original author(s) and the source, provide a link to the Creative Commons licence, and indicate if you modified the licensed material. You do not have permission under this licence to share adapted material derived from this article or parts of it. The images or other third party material in this article are included in the article's Creative Commons licence, unless indicated otherwise in a credit line to the material. If material is not included in the article's Creative Commons licence and your intended use is not permitted by statutory regulation or exceeds the permitted use, you will need to obtain permission directly from the copyright holder. To view a copy of this licence, visit <http://creativecommons.org/licenses/by-nc-nd/4.0/>.

© The Author(s) 2024